

## Article

# Development, Characterization and Valuable Use of Novel Dosimeter Film Based on PVA Polymer Doped Nitro Blue Tetrazolium Dye and AgNO<sub>3</sub> for the Accurate Detection of Low X-ray Doses

Saleh Alashrah <sup>1</sup> , Yassine El-Ghoul <sup>2,3,\*</sup>, Faisal Muteb Almutairi <sup>4</sup> and Mohammed Ahmed Ali Omer <sup>5</sup>

<sup>1</sup> Department of Physics, College of Science, Qassim University, Buraidah 51452, Saudi Arabia; ashrah@qu.edu.sa

<sup>2</sup> Department of Chemistry, College of Science, Qassim University, Buraidah 51452, Saudi Arabia

<sup>3</sup> Textile Engineering Laboratory, University of Monastir, Monastir 5019, Tunisia

<sup>4</sup> College of Science, Al-Imam Muhammad Ibn Saud Islamic University, Riyadh 11623, Saudi Arabia; 381110204@qu.edu.sa

<sup>5</sup> Department of Radiologic Technology, College of Applied Medical Sciences, Qassim University, Buraidah 51452, Saudi Arabia; ma.omer@qu.edu.sa

\* Correspondence: y.elghoul@qu.edu.sa



**Citation:** Alashrah, S.; El-Ghoul, Y.; Almutairi, F.M.; Omer, M.A.A. Development, Characterization and Valuable Use of Novel Dosimeter Film Based on PVA Polymer Doped Nitro Blue Tetrazolium Dye and AgNO<sub>3</sub> for the Accurate Detection of Low X-ray Doses. *Polymers* **2021**, *13*, 3140. <https://doi.org/10.3390/polym13183140>

Academic Editors:  
Domenico Larobina and  
Francesco Nappi

Received: 29 August 2021  
Accepted: 11 September 2021  
Published: 17 September 2021

**Publisher's Note:** MDPI stays neutral with regard to jurisdictional claims in published maps and institutional affiliations.



**Copyright:** © 2021 by the authors. Licensee MDPI, Basel, Switzerland. This article is an open access article distributed under the terms and conditions of the Creative Commons Attribution (CC BY) license (<https://creativecommons.org/licenses/by/4.0/>).

**Abstract:** Currently, the uncontrolled exposure of individuals to X-rays during medical examinations represents a substantial danger that threatens both medical professionals and patients. Therefore, radiation dosimetry for low X-ray doses is a very important control of radiation practice in medical diagnostic radiology. In line with this, the current study proposes a valuable dosimeter-based PVA thin film doubly doped with silver nitrate salt and nitro blue tetrazolium dye. The nanocomposite film was prepared via a simple casting method and the different processing parameters were optimized. The performance of radiation detection was evaluated according to optical, chromic, chemical and structural changes after exposure to variable low X-ray doses (0, 2, 4, 10 and 20 mGy). The different film labels exhibited an excellent stability behavior in dark and light upon 30 days of storage. The UV-Vis spectrophotometric study showed a gradual increase in the maximum absorbance as a function of the dose and the corresponding response curve confirmed this linear variation ( $R = 0.998$ ). A clear structural modification was recorded via X-ray diffraction (XRD) analysis revealing the increase in crystallinity with the level of the dose received by the nanocomposite films. Microscopic surface analysis via SEM assessments revealed a significant morphological change in PVA/Ag<sup>+</sup>/NBT films exposed to increased radiation doses and typical dendrites growing in needle- or tree-like microstructures appeared with a high X-ray dose. Finally, the nanocomposite films before and after irradiation were evaluated via a spectrophotometric study and the different CIELab coordinates, the color difference, as well as the color strength, showed a linear correlation with the intensity of the applied dose. This new dosimeter design could, therefore, provide a promising and efficient alternative for prompt and accurate detection of low X-rays doses in diagnostic radiology.

**Keywords:** PVA nanocomposite film; silver nitrate; nitro blue tetrazolium; characterization; X-ray dosimeter; medical diagnostic radiology

## 1. Introduction

Activities using ionizing radiation are in continuous and considerable evolution. This significant development in various fields may reveal new issues in terms of radiation protection [1,2]. This is particularly the case in the medical sector with the implementation of new techniques using high energy and/or pulsed radiation for radiotherapy as IMRT and hadron therapy or low energy for radiation therapy as interventional and diagnostic radiology [3,4]. These new situations require dosimetric monitoring adapted to the complex

generated fields. At the same time, dosimetric techniques have also evolved, offering, in particular, a larger choice of electronic dosimeters, in particular for neutrons, as well as a diversification of the techniques that can be used (TLD, OSL, RPL) for routine passive dosimetry [5–7].

Irradiation processing is generally investigated for different purposes, such as food irradiation, sterilization of surgical equipment, diagnostic radiology and the polymerization process [8–12]. It is therefore important to take an accurate measurement of the radiation dose delivered over processing. In particular, the precise measurement of low radiation doses remains a problem in view of the absence of effective and appropriate dosimeters even in a very low radiation range [13,14]. Recent advances in the field of dosimetry through the development of photographic films, Geiger-Muller and proportional counters have experienced continuous and rapid progress [15,16]. The investigation of solutions as standards, as well as the variation in oxidation states and color changes, have been extensively studied [17,18]. However, specific manipulations in addition to heavy and expensive instrumentation such as NMR, IR, UV-Vis spectrophotometer, ESR and thermoluminescence are quite necessary for the detection of changes in these solutions. [19,20]. Hence the importance and the necessity of developing simple and practical alternatives capable of detecting and quantifying radiation doses without having recourse to these additional instruments. The simplest solution was through the detection of ionizing radiations via color and shade changes [21,22]. Furthermore, having a lightweight, portable and easy-to-handle dosimeter is very required and advantageous. The most suitable choice was the use of thin films based on different polymers [23,24]. Numerous researches and publications have reported the investigation of polyamide-6, polyvinyl alcohol and polystyrene films doped with various dyes, in the detection of various types of radiation [25–27].

At present, polymers and functional polymers are widely investigated in various fields [28–32]. The doping of various polymers with certain metal ions imparts new and improved properties to the polymer. Indeed, polymers hybridized with transition metals are considered to be versatile materials applied in many scientific fields allowing important industrial technological advances [33–35]. These conductive polymer composites provide the opportunity to enhance their physical, mechanical, electrical and optical properties. These composite metal chelate films based on different polymers such as poly (vinyl alcohol) (PVA), polystyrene (PS) and poly-methyl-methacrylate (PMMA) were reported with their dosimetry control applications [36,37]. The most reported metals studied as a reinforcement of polymer matrix materials, we find, are silver nitrate [38], nickel-oxide [39], bismuth germinate ( $\text{Bi}_4\text{Ge}_3\text{O}_{12}$ -BGO) [40], manganese phthalocyanine [41] and ferrotitanium alloy [42]. The well-studied integration of different metals and dyes in various polymeric matrices could therefore allow practical and efficient dosimeters. Their performance is manifested by remarkable changes in physical, optical, colorimetric, structural and electrical properties after exposure to various irradiation dose levels. Plastic-films-based PVA polymers are well-reported and studied in various dosimetric applications [43,44]. PVA is the most convenient for the development of dosimetric films thanks to its low cost, water-solubility, ease of availability and possibility to incorporate a wide range of metal salts and dyes, in addition to its ability to be easily cast at moderately low temperatures. The nitro tetrazolium blue dye is previously reported by our group as an efficient indicator of low radiation doses. Its compatibility with PVA polymer is conducive to the development of a practical and effective dosimeter [45]. The investigation of  $\text{AgNO}_3$  with PVA thin film has demonstrated the easy formation of polymer metal chelate and the resulting film exhibited promising performance and sensitivity to low radiation doses [46].

The current study aims to take advantage of a double matrix filling using both dyes and metals to prepare an efficient composite film dosimeter based on PVA polymer and doped with silver nitrate and nitro blue tetrazolium dye. Faced with the scarcity of research on the study of hybridized polymeric dosimeters, which are effective for the detection and the quantification of low radiation doses (in mGy dose level), our versatile dosimeter represents a real challenge finding its practical importance in medical diagnostic radiology.

A simple casting method will be performed to synthesize the PVA nanocomposite thin film-based nitrate chelate and NBT dye. Different parameters of the film processing were preliminarily optimized including the concentration, time and temperature of preparation. Different X-rays doses (0, 2, 4, 10 and 20 mGy) were then applied to the synthesized films. Afterward, chemical, structural, physical and morphological characterizations via UV, XRD and SEM analysis were performed on the raw and exposed films. In addition, the colorimetric properties of the irradiated films were evaluated in order to assess the efficiency and the sensitivity performance of these developed dosimeters. Furthermore, the determination of the various curves illustrating the responses, resulting from the various mentioned characterizations, according to the increasing doses applied to PVA/Ag<sup>+</sup>/NBT nanocomposite films was carried out to evaluate the performance of the dosimeter in the field of X-ray diagnostic radiology.

## 2. Experiment

### 2.1. Materials

The silver nitrate (AgNO<sub>3</sub>, M<sub>w</sub> = 169.87 g/mol) and nitro blue tetrazolium chloride (C<sub>40</sub>H<sub>30</sub>Cl<sub>2</sub>N<sub>10</sub>O<sub>6</sub>·H<sub>2</sub>O·CH<sub>4</sub>O; M<sub>w</sub> = 867.70) investigated as matrix reinforcements for the different dosimetric films, as well as the polyvinyl alcohol polymer (PVA, M<sub>w</sub> = 85–124 kDa with a hydrolysis degree of 85–90%), were acquired from Sigma Aldrich (St. Louis, MO, USA). Ultrapure water (Milli-Q<sup>®</sup> Direct, Darmstadt, Germany), was used for the preparation of the film nanocomposites. All reagents employed were of analytical grade and were used in the various experiments without further purification.

### 2.2. Characterization of Film Nanocomposites

The synthesized nanocomposite films were characterized via different techniques and the comparison between the raw and irradiated films at various doses was beneficial for the evaluation of the efficiency of the films as low X-ray radiation dosimeters.

FTIR analysis via the attenuated total reflection (ATR) method was carried out for the determination of various spectra of raw and irradiated films using an infrared spectrophotometer (Agilent Technologies/Gladi-ATR, Santa Clara, CA, USA). A range scale varied from 4000 to 400 cm<sup>-1</sup> and a resolution of 4 cm<sup>-1</sup> were fixed for the measurement of different infrared spectra.

A UV–vis spectrophotometer (Shimadzu, UV-2501PC, Kyoto, Japan) was investigated for the measurement of the absorption curves of different film labels. The measurements were carried out on a scale of wavelength varying from 200 to 700 nm.

An X-ray Diffractometer (PW 1720 Philips) was used to obtain the X-ray diffraction patterns. The samples were scanned at the 2θ angle varying from 10° to 90°. The step width was 0.01°. The operating voltage and current intensity were 40 kV and 40 mA, respectively.

The mechanical study was performed using a Universal Testing Machine (Zwick Testing Machine Ltd., Leomister, UK). Film samples were cut as 5 mm × 40 mm. A crosshead speed of 5 mm/min was set throughout the experiment. The measurements were carried out according to the standard ASTM D638 at 22 °C with 65% relative humidity. Each measurement was an average of five replicates.

The morphological study of the surface of raw and X-ray exposed films was accomplished via SEM analysis. Different SEM micrographs were obtained using Scanning Electron Microscopy (JEOL JSM-5400 LV, JEOL Ltd., Akishima, Japan). A 5 kV acceleration voltage was selected during measurements. Magnifications were varied from 100 to 2000×. In order to improve surface conductivity, all samples were subjected to a surface coating of a thin layer of Au before analysis.

The evaluation of colorimetric characteristics of raw and irradiated films was carried out using a spectrophotometer instrument (3NH-YD5010) operating in the visible spectrum

at 39 wavelengths in a wavelength range varying from 380 to 780 nm. The color strength (K/S) values were measured using the equation of Kubelka–Munk Equation (1) [47].

$$\left(\frac{K}{S}\right)_\lambda = \frac{(1 - R_\lambda)^2}{2 \times R_\lambda} \quad (1)$$

where K is the absorption coefficient, S is the scattering factor and  $R_\lambda$  represents the spectral reflectance of the colored film at  $\lambda_{\max}$  [48].

The different CIELab color coordinates of PVA/Ag/NBT nanocomposite films ( $L^*$ ,  $a^*$ ,  $b^*$ ) and the  $\Delta E$  variation representing the color total difference were measured under a standard observer of  $10^\circ$  and the daylight standard illuminant  $D_{65}$ .  $L^*$  represents the lightness coordinate,  $a^*$  and  $b^*$  describe the redness-greenness and the yellowness-blueness axis, respectively [49,50].

The  $\Delta E$  values were calculated as a function of the various measured color coordinates as following (Equation (2)).

$$\Delta E = \sqrt{(L^* - L_0)^2 + (a^* - a_0)^2 + (b^* - b_0)^2} \quad (2)$$

where ( $L^*$ ,  $a^*$ ,  $b^*$ ) and ( $L_0$ ,  $a_0$ ,  $b_0$ ) are the measured CIELab coordinates for the raw and irradiated PVA/Ag/NBT films, respectively. The average limit of the distance  $\Delta E$  between two CIELab coordinates is the value above which the human eye cannot differentiate. Many limits of  $\Delta E$  depending mainly on color saturation have already been reported in various research works [51,52].

### 2.3. Preparation of PVA/NBT Nanocomposite Films

The films-based PVA polymers mixed with various amounts of NBT and silver nitrate fillers were developed following a previously reported casting method in our laboratory [45]. A 5% solution of PVA dissolved in distilled water was prepared. The bulk solution was then heated gently, using a heater instrument with controlled temperature. The preparation was kept under continuous stirring at a constant temperature of  $80^\circ\text{C}$ . After 2 h, the polymer solution was cooled, to an ambient temperature and two prepared solutions of NBT (0.04% dissolved in 10 mL of ethanol) and  $\text{AgNO}_3$  (0.04% dissolved in 10 mL of distilled water) were poured in the viscous clear solution of PVA. After 1 h of stirring without heating, 20 mL of the solution was poured in glass petri dishes. The dishes were then set to dry in dark (to avoid direct exposure to light) at room temperature for 3 days. The thickness of peeled films was then measured using a thickness numerical instrument. The mean value of the thickness of films was around  $100\ \mu\text{m}$ . The nanocomposite films were finally cut into small pieces of 2 cm sides and stored in black envelopes away from any light to avoid their possible deterioration and to achieve thermal equilibrium before their next use.

A digital X-ray fluoroscopic machine (GE, healthcare, model A101CII, Chicago, USA) was used for the irradiation of different films with variable selected doses. This fluoroscopic device was programmed by adjusting the various technical exposure factors (kVp = 60, mAs = 16 and at 100 cm) thus producing the desired exposure doses of x, y, z mGy. The system was calibrated and verified via an ionization chamber to generate the appropriate doses.

## 3. Results and Discussion

### 3.1. Post-Irradiation Stability

PVA/Ag<sup>+</sup>/NBT prepared films and treated with a dose of 20 mGy were stowed in light and dark at an ambient temperature. The storage of different films was for 30 days. The absorbance at 460 nm was determined during this storage at varying time intervals. The variation of the maximum absorbance of the irradiated nanocomposite films measured as a function of the storage period in light and in dark is presented in Figure 1.

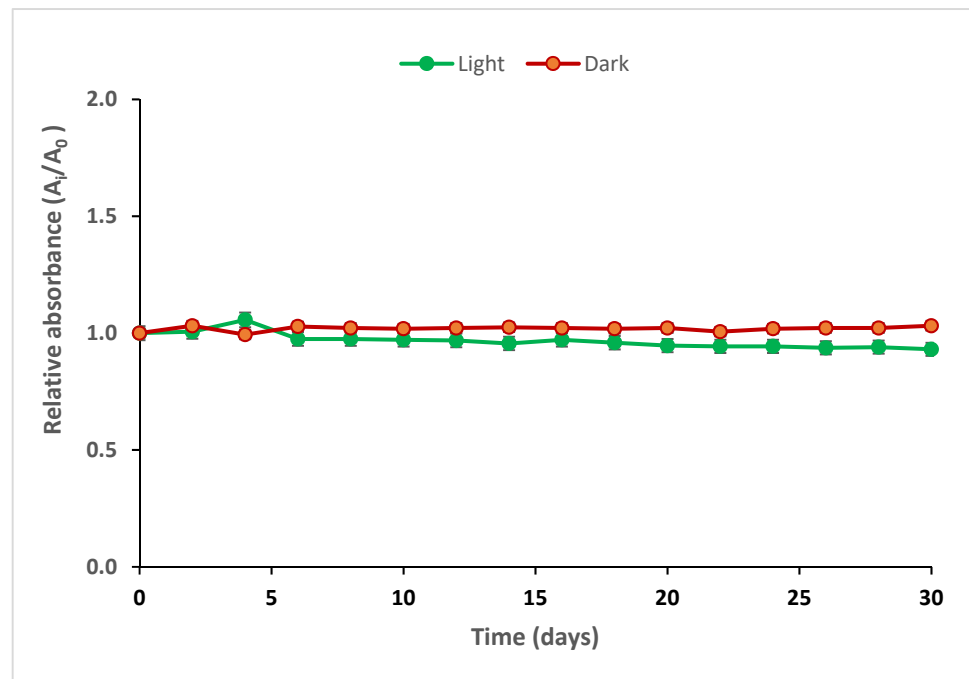


**Figure 1.** Post-irradiation stability of PVA/Ag<sup>+</sup>/NBT films after exposure to an X-ray dose of 20 mGy.

Figure 1 shows the excellent stability of the different films stored at variable times. Irradiated nanocomposite films exhibited good stability both in light and dark storage conditions for 30 days.

This confirmed stability of the PVA/Ag<sup>+</sup>/NBT nanocomposite films is important for practical dosimeters and more effective than other reported film dosimeters consisting only of PVA and silver nitrate or the PVA/NBT in solution or gel form [53,54]. This is due to the rigidity of the compact form of the casted film and the good compatibility between PVA, the organic dye and the metal chelate. The homogenous mixture of these three protagonists provided the nanocomposite film with excellent crystalline properties.

### 3.2. Direct Perception of Color Change after Irradiation

A significant color deviation was directly perceived with eyes after irradiation of the different nanocomposite thin films. Figure 2, reveals a gradual color change according to the intensity of the X-ray dose. The color deviation gradually evolves with the dose from a yellow for unirradiated film to a dark yellowish brown shade. The color modification is related to the reduction of NBT<sup>2+</sup> to mono-formazan (MF<sup>+</sup>) then to a stable hydrophobic di-formazan (DF) structure [55] and also due to the reduction of silver ions in the PVA metal chelate complex into metallic silver Ag<sup>0</sup> [56]. The two PVA matrix fillers exhibited the ability to induce a color change after irradiation. These changes in shade detected following irradiations of very low doses prove well the high sensitivity of these developed dosimeters and thus they are effective for the precise control of the doses in diagnostic radiology.



**Figure 2.** Direct perceived color change of PVA/Ag<sup>+</sup>/NBT films irradiated with different X-ray doses.

### 3.3. UV/Visible Absorption Spectra

The absorption spectra of irradiated PVA/Ag<sup>+</sup>/NBT films were measured in the wavelength range of 200–800 nm. The raw un-irradiated film was considered a reference. The different absorption spectra of nanocomposite films were recorded at variable X-ray doses. The film gradually turns dark yellowish-brown after X-ray irradiation. Absorption spectra of different PVA/Ag<sup>+</sup>/NBT films show in Figure 3 a wide peak centered at 462 nm. The absorption intensity of the peaks at this wavelength increased progressively according to increasing X-ray doses. This gradual increase shows, throughout, that the trends of the curves are related to the reduction of NBT<sup>2+</sup> to mono-formazan (MF<sup>+</sup>) then to a stable hydrophobic di-formazan (DF) structure [57,58] and also due to the reduction of silver ions in the PVA metal chelate complex into metallic silver Ag<sup>0</sup> [59,60] under the effect of the applied irradiation. This change in absorption behavior in the visible region after irradiation is manifested also by the modification in perceived color. Indeed, under the effect of radiation the color undergoes a deviation from yellow to dark yellowish-brown after reduction of NBT [57,58] and from yellow to dark green following the reduction of silver [61]. Moreover, the maximum absorption of the different spectra gradually shifted, with the increase in X-ray doses, from 462 to 472 nm (with a dose of 20 mGy). This was probably due to the more prominent reduction of both Ag<sup>+</sup> ions providing Ag<sup>0</sup> and formazan for the NBT thus allowing the di-formazan product.

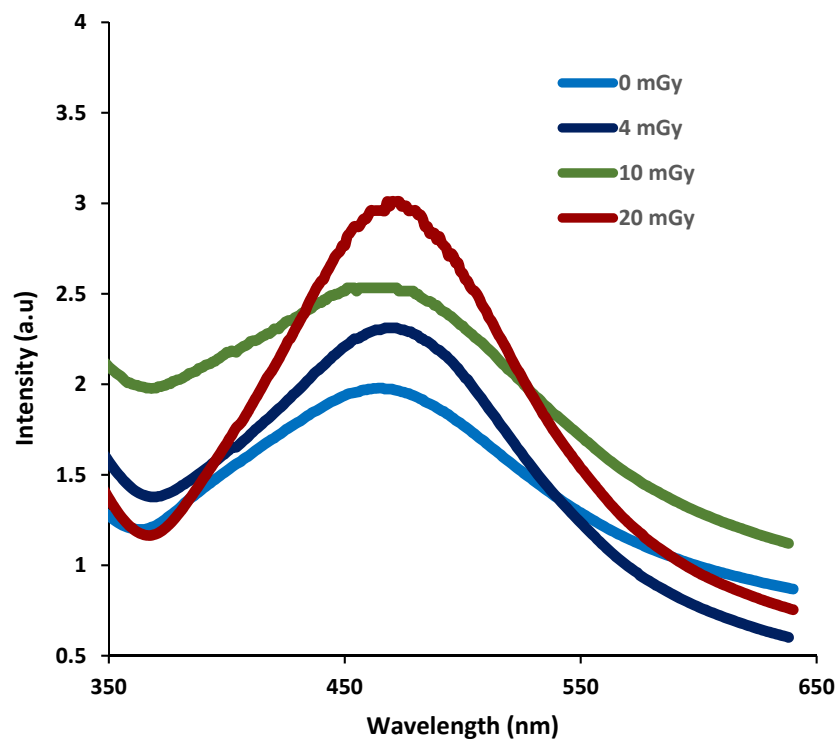


**Figure 3.** UV-Vis spectra of PVA/Ag<sup>+</sup>/NBT nanocomposite films before and after exposure to increased X-ray doses.

### 3.4. Response Curve

Figure 4 shows the variation in absorbance capacity as a function of the increase in the applied X-ray dose. This dose response curve revealed a perfect correlation with the intensity of the dose and the variation is practically linear presenting a coefficient of linear regression  $R = 0.998$ . This perfect correlation is very significant in the application of PVA/Ag<sup>+</sup>/NBT thin films as effective dosimeters in the detection and quantification of low X-ray doses.

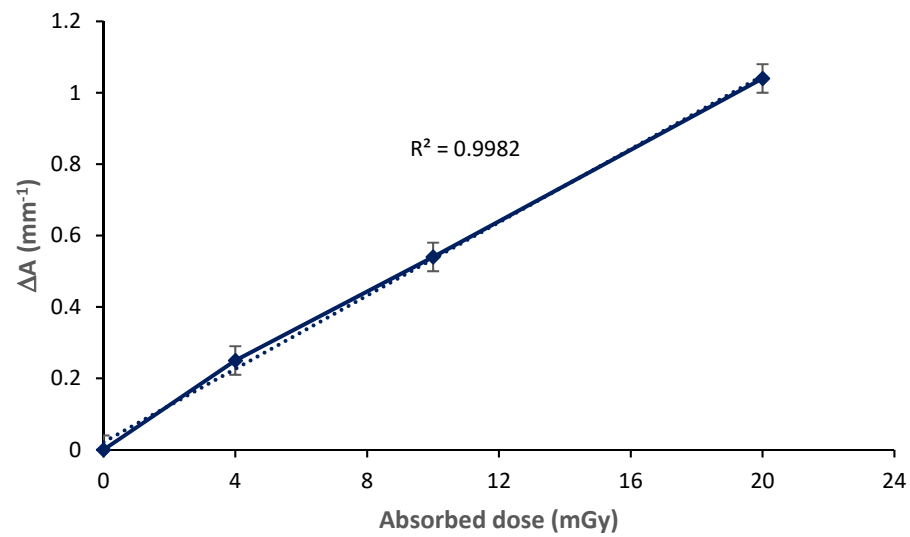


**Figure 4.** Dose–response curve based on UV-Vis absorption capacities at  $\lambda_{\text{max}}$  for PVA/Ag<sup>+</sup>/NBT films exposed at various X-ray doses.

### 3.5. X-ray Diffraction Study

The X-ray exposure could generate some structural changes that are detectable by XRD analysis. XRD characterization was conducted to assess the different structural modifications and rearrangements revealed in the XRD diffractograms due to X-radiation treatment of the nanocomposite films with increased doses. As shown in Figure 5, the different prominent peaks in XRD patterns were well in agreement with the literature values [62]. XRD diffractogram of the unirradiated sample divulges the presence of a characteristic peak centered at  $2\theta = 16.6^\circ$ , which was ascribed to the diffraction plane (00 $\bar{1}$ ) of PVA. This peak, referring to the amorphous state, disappeared after irradiation treatment. Furthermore, XRD patterns show a principal peak at  $2\theta = 19.64^\circ$  which is assigned to the diffraction from a mixture of planes (101) and (10 $\bar{1}$ ) [63]. This peak shifts to the higher angle side from control to irradiated films. In addition, we noticed the decrease in the intensity of this important diffraction peak with the increase in the X-ray irradiation dose implying the decrease in the crystallinity of treated films. This result confirmed the presence of an obvious structural rearrangement in the polymer matrix varying with the intensity of the applied dose.

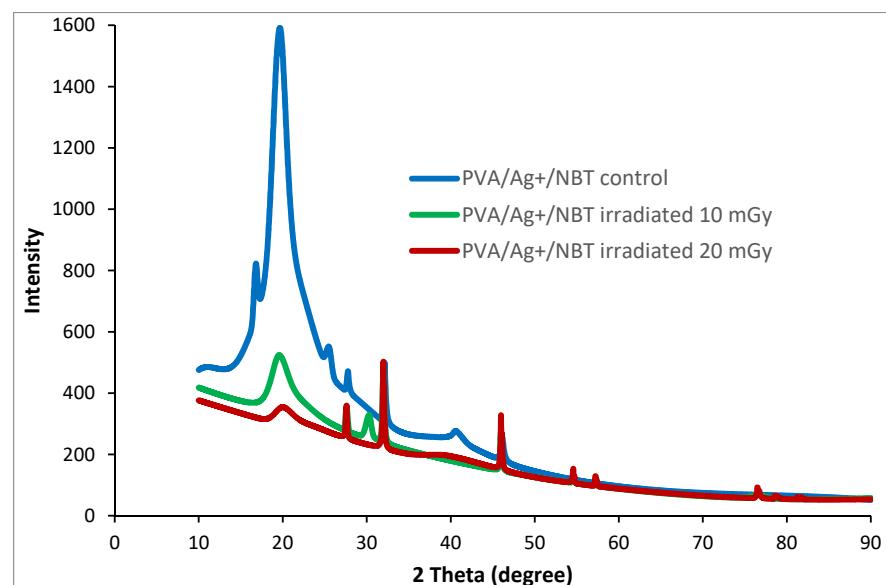


**Figure 5.** XRD patterns of control and irradiated PVA/Ag<sup>+</sup>/NBT nanocomposite films.



### 3.6. Mechanical Characterization

Figure 6 shows the variation of the tensile strength of the PVA film, as well as untreated and irradiated PVA/Ag<sup>+</sup>/NBT nanocomposite films. We noticed a relatively significant increase in tensile strength after the incorporation of NBT and Ag into the matrix of the nanocomposite film. Therefore, this confirmed the absence of phase separation on the doped film, thus indicating good compatibility between NBT, silver and PVA, which improved the tear-resistance of the made composite film. This phenomenon can be caused by the presence of hydrogen and coordination bonds which enhance the intermolecular forces between the NBT, the silver and the base PVA matrix and thus improve the tensile strength of the PVA blend film [64]. With increased X-ray doses, the tensile strength decreased slightly. This confirmed the reduction of the crystalline structure after irradiation (confirmed from XRD analysis). The decrease in mechanical properties suggests that irradiation induces structural rearrangement and probably the prevalence of intermolecular and chain scission processes.

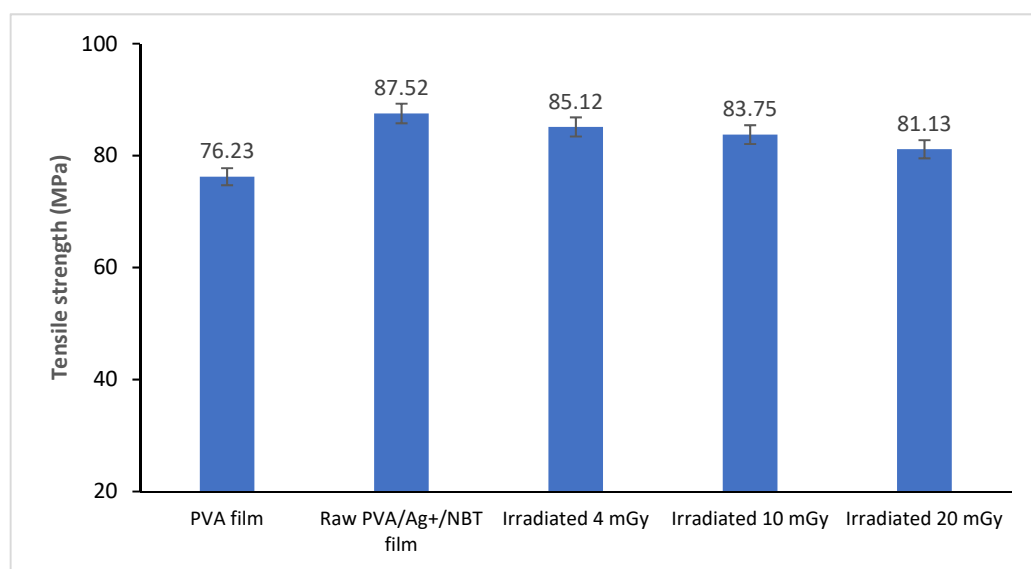


**Figure 6.** Tensile strength variation of raw PVA film, control and irradiated PVA/Ag<sup>+</sup>/NBT nanocomposite films with increased X-ray doses.

### 3.7. SEM Morphological Analysis

Control and treated samples with various X-ray doses were characterized by SEM analysis to assess the effect of different radiation doses on the surface morphology and microstructure of exposed nanocomposite films. Concerning the non-irradiated film, Figure 7a shows a uniform, smooth homogeneous and compact microstructure without any phase separation thus showing the excellent compatibility of the various protagonists of the PVA matrix [65]. We notice after radiation treatment a clear modification of the morphology of the exposed films with the appearance of some fluke-like structures and many surface stripes (Figure 7b,c). The surface degradation is all the more pronounced and intense with the increased X-ray doses. An alteration manifested by a significant microstructural change is illustrated by regular forms of cracks extending in all directions (Figure 7d,e,f). These micrographs at increased magnifications show dendritic characters with a clear main trunk and side branches. Dendrite growth occurs as a result of the reduction of metal ions dissolved in the nanocomposite film, thereby growing in needle- or tree-like microstructures [66]. This form of degradation detected in the film after irradiation could therefore be specific to our nanocomposite film, thus offering more specificity and performance to this dosimeter designed for low doses of X-rays.



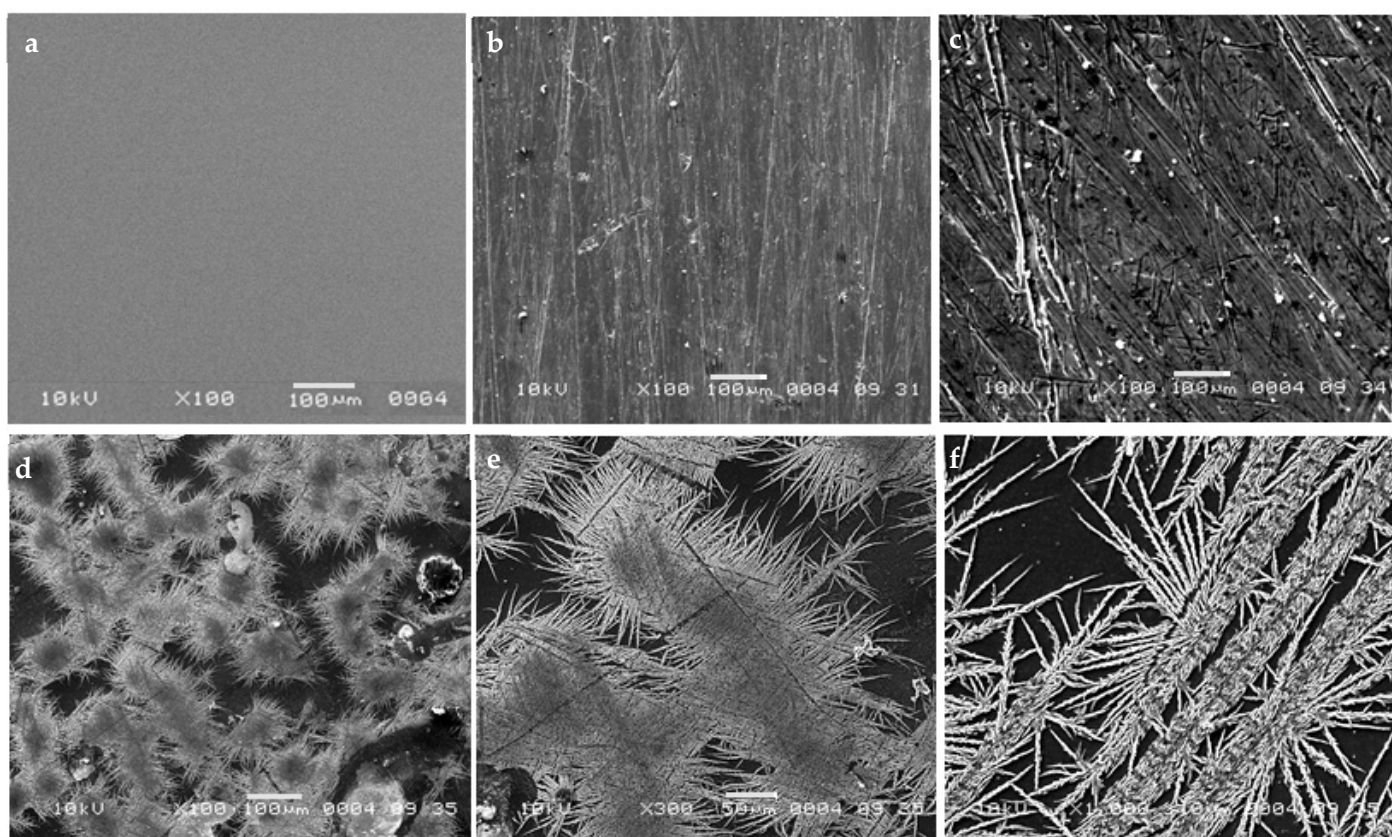


**Figure 7.** SEM micrographs of PVA/Ag<sup>+</sup>/NBT control film (a) and irradiated PVA/Ag<sup>+</sup>/NBT films with 4 mGy (b), 10 mGy (c) and 20 mGy with different magnifications (d–f).

### 3.8. Colorimetric Study

The color deviation in intensity or shade after irradiation is a crucial property of an effective dosimeter. The performance becomes more practical when the color change varies with dose and is easily perceived by the human eye. A spectrophotometric study was carried out to assess and quantify the color variation of the PVA/Ag<sup>+</sup>/NBT nanocomposite films after their irradiation with increased low X-ray doses. The mean deviation of the CIELab coordinates L\*, a\*, b\*, the total color difference ( $\Delta E$ ) and the color strength (K/S) evaluations for the control and the irradiated PVA/Ag<sup>+</sup>/NBT prepared films are presented in Table 1.

**Table 1.** CIELab coordinates (L\*, a\*, b\*),  $\Delta E$  and K/S measurements for control and irradiated PVA/Ag<sup>+</sup>/NBT films from 4 to 20 mGy.

Radiation Dose	L*	a*	b*	$\Delta E$	K/S
0	51.61	2.04	12.14	-	4.11
4	52.80	2.28	13.44	10.47	4.47
10	54.90	2.81	15.27	13.05	4.76
20	57.73	3.65	17.83	16.73	5.30

The different measurements of the three color coordinates in the CIELab space, L\*, a\* and b\* according to the X-ray dose irradiating the various treated films, are presented in Figure 8a–c. The tendency of the lightness (L\*) curve decreases linearly with increasing treatment dose, this means that the color becomes darker and darker. However, the Cartesian color coordinates a\*, b\* increased with the intensity of the applied dose, this means that the color of the films is more reddish and bluish. The variations measured via the spectrophotometer clearly show a perfect correlation between each color parameter and

the intensity of the applied dose. The linear dependence of the different color coordinates according to the increased applied radiation dose allows each color's coordinate  $a^*$ ,  $b^*$  and  $L^*$  to be investigated separately as a dosimetric index for low dose radiation varying from 0 to 20 mGy. Furthermore, Figure 8d shows the perfect increase of the  $\Delta E$  (representing the total color deviation) with the intensity of X-ray treatment doses. This total color difference for all the doses is much higher than 1 (from 3.5 to 9.5) so the color change is clearly perceptible with the human eye. The  $\Delta E$  values vary linearly with increased doses applied to the different samples. The same tendency was observed for K/S (color strength). This important color parameter increased quasi-linearly with higher radiation doses (Figure 8e). The spectroradiometry study revealed well the efficiency of the designed nanocomposite PVA/Ag<sup>+</sup>/NBT thin film as a performance irradiation indicator. The direct perceived change in color reflects well the potential of this dosimetric system to control low radiation in diagnostic radiology.

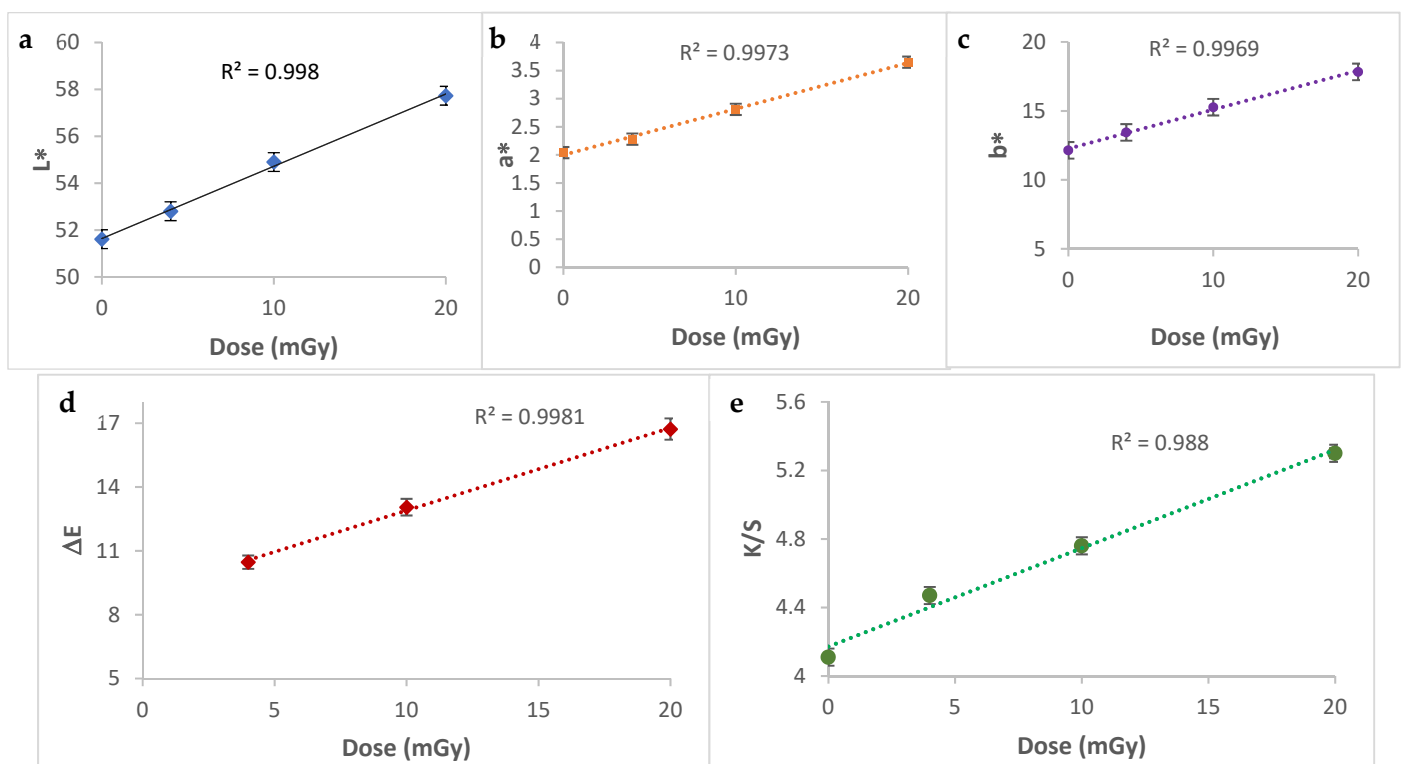


**Figure 8.** CIELab color parameters ( $L^*$ ,  $a^*$  and  $b^*$ ) (a–c), total color difference ( $\Delta E$ ) (d) and color strength (K/S) (e) measurements for PVA/Ag<sup>+</sup>/NBT films irradiated from 4 to 20 mGy.

#### 4. Conclusions

The accurate evaluation of the X-ray dose to the patient is an essential aspect of the control process in X-ray diagnostic radiology. Therefore, it is a crucial necessity to develop an effective dosimetric system for the accurate evaluation and quantification of the X-radiation in diagnostic radiology examinations. In this study, we developed a new designed dosimetric film-based PVA polymer doped with both silver nitrate salt and NBT dye. The performance of the nanocomposite film has been confirmed via the different applied characterizations after increased radiation treatments. Indeed, the absorption capacity varied linearly with the intensity of the X-ray doses. This was due to the reduction of NBT<sup>2+</sup> to mono-formazan and di-formazan form and the reduction in the same time of the silver ion Ag<sup>+</sup> in the polymer metal chelate to Ag<sup>0</sup>, under the effect of the X-ray treatment. XRD assessment via the investigation of the different patterns revealed significant structural modification and crystallinity change after various radiation exposures. SEM analysis showed a clear morphological modification of PVA/Ag<sup>+</sup>/NBT thin films after

X-ray treatment depending on the applied dose, confirming thus the high sensitivity of the dosimetry films upon very low doses. Furthermore, the different developed thin films exhibited excellent post-irradiation stability in light and dark from 5 to 30 days after X-ray exposure. The spectrophotometric study was the most important in view of the practical impact of a color change after irradiation exposure. All color parameters showed linear quantitative (measured coordinates) and qualitative (direct perception of color) variation with increasing treatment dose. Moreover, the total color difference and the color strength were also shown to be linearly increased with augmented radiation doses. The various characterization assessments confirmed the excellent radiation detection via the designed nanocomposite films exposed to very low radiation doses (in the mGy scale). The developed polymeric nanocomposite film has shown practical efficiency as a new potential irradiation indicator for routine diagnostic control processes.

**Author Contributions:** Data curation, S.A., Y.E.-G., F.M.A., and M.A.A.O.; Formal analysis, S.A., Y.E.-G., F.M.A., and M.A.A.O.; Investigation, S.A., Y.E.-G.; Methodology, Y.E.-G. and S.A.; Project administration, S.A. and Y.E.-G.; Software, S.A., F.M.A., and Y.E.-G.; Supervision, S.A.; Validation, S.A., F.M.A., and Y.E.-G.; Writing—original draft, S.A., Y.E.-G.; Writing—review and editing, Y.E.-G. All authors have read and agreed to the published version of the manuscript.

**Funding:** The authors gratefully acknowledge Qassim University, represented by the Deanship of Scientific Research, on the financial support for this research under the number 5677-cos-2019-2-2-I, during the academic year 1440 AH/2019 AD.

**Institutional Review Board Statement:** Not applicable.

**Informed Consent Statement:** Not applicable.

**Conflicts of Interest:** The authors declare no conflict of interest.

## References

1. Mohammadi, M. Book review: Advanced Radiation Protection Dosimetry edited by Shaheen A. Dewji and Nolan E. Hertel. *Phys. Eng. Sci. Med.* **2020**, *43*, 727–728. [[CrossRef](#)]
2. Alevra, A.V.; Klein, H.; Knauf, K.; Wittstock, J. Neutron field spectrometry for radiation protection dosimetry purposes. *Radiat. Prot. Dosim.* **1992**, *44*, 223–226. [[CrossRef](#)]
3. Alterio, D.; D'Ippolito, E.; Vischioni, B.; Fossati, P.; Gandini, S.; Bonora, M.; Ronchi, S.; Vitolo, V.; Mastella, E.; Magro, G.; et al. Mixed-Beam Approach in Locally Advanced Nasopharyngeal Carcinoma: IMRT Followed by Proton Therapy Boost Versus IMRT-Only. Evaluation of Toxicity and Efficacy. *Acta Oncol.* **2020**, *59*, 541–548. [[CrossRef](#)] [[PubMed](#)]
4. Guardiola, C.; Fleta, C.; Quirion, D.; Pellegrini, G.; Gómez, F. Silicon 3D Microdetectors for Microdosimetry in Hadron Therapy. *Micromachines* **2020**, *11*, 1053. [[CrossRef](#)]
5. Bhatt, B.C.; Kulkarni, M.S. Worldwide Status of Personnel Monitoring using Thermoluminescent (TL), Optically Stimulated Luminescent (OSL) and Radiophotoluminescent (RPL) Dosimeters. *Int. J. Lumin. Appl.* **2013**, *3*, 6–10.
6. Pradhan, A.S.; Lee, J.I.; Kim, J.L. On the scenario of passive dosimeters in personnel monitoring: Relevance to diagnostic radiology and fluoroscopy-based interventional cardiology. *J. Med. Phys.* **2016**, *41*, 81–84. [[CrossRef](#)]
7. Wesolowska, P.E.; Cole, A.; Santos, T.; Bokulic, T.; Kazantsev, P.; Izewska, J. Characterization of three solid state dosimetry systems for use in high energy photon dosimetry audits in radiotherapy. *Radiat. Meas.* **2017**, *106*, 556–562. [[CrossRef](#)]
8. Pati, S.; Chatterji, A.; Dash, B.P.; Raveen Nelson, B.; Sarkar, T.; Shahimi, S.; Atan Edinur, H.; Binti Abd Manan, T.S.; Jena, P.; Mohanta, Y.K.; et al. Structural Characterization and Antioxidant Potential of Chitosan by  $\gamma$ -Irradiation from the Carapace of Horseshoe Crab. *Polymers* **2020**, *12*, 2361. [[CrossRef](#)] [[PubMed](#)]
9. Hu, J.; Zhang, M.; He, Y.; Zhang, M.; Shen, R.; Zhang, Y.; Wang, M.; Wu, G. Fabrication and Potential Applications of Highly Durable Superhydrophobic Polyethylene Terephthalate Fabrics Produced by In-Situ Zinc Oxide (ZnO) Nanowires Deposition and Polydimethylsiloxane (PDMS) Packaging. *Polymers* **2020**, *12*, 2333. [[CrossRef](#)]
10. Tapia-Guerrero, Y.S.; Del Prado-Audelo, M.L.; Borbolla-Jiménez, F.V.; Giraldo Gomez, D.M.; García-Aguirre, I.; Colín-Castro, C.A.; Morales-González, J.A.; Leyva-Gómez, G.; Magaña, J.J. Effect of UV and Gamma Irradiation Sterilization Processes in the Properties of Different Polymeric Nanoparticles for Biomedical Applications. *Materials* **2020**, *13*, 1090. [[CrossRef](#)] [[PubMed](#)]
11. Peng, Y.K.; Lui, C.N.P.; Chen, Y.W.; Chou, S.W.; Raine, E.; Chou, P.T.; Yung, K.K.L.; Tsang, S.C.E. Engineering of Single Magnetic Particle Carrier for Living Brain Cell Imaging: A Tunable T1-/T2-/Dual-Modal Contrast Agent for Magnetic Resonance Imaging Application. *Chem. Mater.* **2017**, *29*, 4411–4417. [[CrossRef](#)]
12. Li, C.H.; Kuo, T.R.; Su, H.J.; Lai, W.Y.; Yang, P.C.; Chen, J.S.; Wang, D.Y.; Wu, Y.C.; Chen, C.C. Fluorescence-Guided Probes of Aptamer-Targeted Gold Nanoparticles with Computed Tomography Imaging Accesses for in Vivo Tumor Resection. *Sci. Rep.* **2015**, *5*, 15675. [[CrossRef](#)]



13. Inaba, Y.; Nakamura, M.; Zuguchi, M.; Chida, K. Development of Novel Real-Time Radiation Systems Using 4-Channel Sensors. *Sensors* **2020**, *20*, 2741. [[CrossRef](#)]
14. Phong Vo, P.; Ngoc Doan, H.; Kinashi, K.; Sakai, W.; Tsutsumi, N.; Phu Huynh, D. X-ray Visualization and Quantification Using Fibrous Color Dosimeter Based on Leuco Dye. *Appl. Sci.* **2020**, *10*, 3798. [[CrossRef](#)]
15. Diffey, B. The Early Days of Personal Solar Ultraviolet Dosimetry. *Atmosphere* **2020**, *11*, 125. [[CrossRef](#)]
16. Kržanović, N.; Stanković, K.; Živanović, M.; Đaletić, M.; Ciraj-Bjelac, O. Development and testing of a low cost radiation protection instrument based on an energy compensated Geiger-Müller tube. *Radiat. Phys. Chem.* **2019**, *164*, 108358. [[CrossRef](#)]
17. Glais, E.; Massuyeau, F.; Gautier, R. Tuning the oxidation states of dopants: A strategy for the modulation of material photoluminescence properties. *Chem. A Eur. J.* **2020**, *27*, 905–914. [[CrossRef](#)]
18. William, J.E. Tutorial on the Role of Cyclopentadienyl Ligands in the Discovery of Molecular Complexes of the Rare-Earth and Actinide Metals in New Oxidation States. *Organometallics* **2016**, *35*, 3088–3100.
19. Bhaskar, S.; Goswami, M.; Shobha, S.; Prakasan, V.; Krishnan, M.; Ghosh, S.K. Thermoluminescence and electron paramagnetic resonance study on rare earth/transition metal doped lithium borate glasses for dosimetry applications. *J. Lumin.* **2019**, *216*, 116725.
20. Chandler, J.R.; Sholom, S.; McKeever, S.W.S.; Hall, H.L. Thermoluminescence and phototransferred thermoluminescence dosimetry on mobile phone protective touchscreen glass. *J. Appl. Phys.* **2019**, *126*, 074901. [[CrossRef](#)]
21. Vo, P.P.; Doan, H.N.; Kinashi, K.; Sakai, W.; Tsutsumi, N. X-ray composite fibrous color dosimeter based on 10,12-pentacosadiynoic acid. *Dyes Pigments* **2021**, *191*, 109356. [[CrossRef](#)]
22. AL Zahran, A.; Rabaeh, K.; Eyadeh, M.; Basfar, A. Dosimetric evaluation of methyl red radiochromic film for radiation processing. *Pigment. Resin Technol.* **2020**, *50*, 157–162. [[CrossRef](#)]
23. Ozkan Loch, C.; Eichenberger, M.A.; Togno, M.; Zinsli, S.P.; Egloff, M.; Papa, A.; Ischebeck, R.; Lomax, A.J.; Peier, P.; Safai, S. Characterization of a Low-Cost Plastic Fiber Array Detector for Proton Beam Dosimetry. *Sensors* **2020**, *20*, 5727. [[CrossRef](#)]
24. Santos, T.; Ventura, T.; Lopes, M.d.C. A review on radiochromic film dosimetry for dose verification in high energy photon beams. *Radiat. Phys. Chem.* **2020**, *179*, 109217.
25. Sasiadek, E.; Jaszczak, M.; Skwarek, J.; Kozicki, M. NBT-Pluronic F-127 Hydrogels Printed on Flat Textiles as UV Radiation Sensors. *Materials* **2021**, *14*, 3435. [[CrossRef](#)] [[PubMed](#)]
26. Seito, H.; Ichikawa, T.; Hanaya, H.; Sato, Y.; Kaneko, H.; Haruyama, Y.; Watanabe, H.; Kojima, T. Application of clear polymethylmethacrylate dosimeter Radix W to a few MeV electron in radiation processing. *Radiat. Phys. Chem.* **2009**, *78*, 961–965. [[CrossRef](#)]
27. Rabaeh, K.A.; Basfar, A.A. A polystyrene film dosimeter containing dithizone dye for high dose applications of gamma-ray source. *Radiat. Phys. Chem.* **2020**, *170*, 108646. [[CrossRef](#)]
28. Alminderej, F.M.; Ammar, C.; El-Ghoul, Y. Functionalization, characterization and microbiological performance of new biocompatible cellulosic dressing grafted chitosan and Suaeda fruticosa polysaccharide extract. *Cellulose* **2021**. [[CrossRef](#)]
29. EL-Ghoul, Y.; Ammar, C.; Alminderej, F.M.; Shafiquzzaman, M. Design and Evaluation of a New Natural Multi-Layered Biopolymeric Adsorbent System-Based Chitosan/Cellulosic Nonwoven Material for the Biosorption of Industrial Textile Effluents. *Polymers* **2021**, *13*, 322. [[CrossRef](#)]
30. Ammar, C.; Alminderej, F.M.; EL-Ghoul, Y.; Jabli, M.; Shafiquzzaman, M. Preparation and Characterization of a New Polymeric Multi-Layered Material Based K-Carrageenan and Alginate for Efficient Bio-Sorption of Methylene Blue Dye. *Polymers* **2021**, *13*, 411. [[CrossRef](#)]
31. El-Ghoul, Y. Biological and microbiological performance of new polymer-based chitosan and synthesized aminocyclodextrin finished polypropylene abdominal wall prosthesis biomaterial. *Text. Res. J.* **2020**, *90*, 2690–2702. [[CrossRef](#)]
32. Alminderej, M.F.; El-Ghoul, Y. Synthesis and study of a new biopolymer-based chitosan/hematoxylin grafted to cotton wound dressings. *J. Appl. Polym. Sci.* **2019**, *136*, 47625. [[CrossRef](#)]
33. Dhibar, S.; Sahoo, S.; Das, C.K. Fabrication of transition-metal-doped polypyrrole/multiwalled carbon nanotubes nanocomposites for supercapacitor applications. *J. Appl. Polym. Sci.* **2013**, *130*, 554–556. [[CrossRef](#)]
34. Carraro, M.; Gross, S. Hybrid Materials Based on the Embedding of Organically Modified Transition Metal Oxoclusters or Polyoxometalates into Polymers for Functional Applications: A Review. *Materials* **2014**, *7*, 3956–3989. [[CrossRef](#)] [[PubMed](#)]
35. Ueda, K.; Kakuta, T.; Tanaka, K.; Chujo, Y. High Refractive-Index Hybrids Consisting of Water-Soluble Matrices with Bipyridine-Modified Polyhedral Oligomeric Silsesquioxane and Lanthanoid Cations. *Polymers* **2020**, *12*, 1560. [[CrossRef](#)] [[PubMed](#)]
36. Khanna, P.K.; Singh, N.; Charan, S.; Viswanath, K.A. Synthesis of Ag/polyaniline nano composite via an in situ photo-redox mechanism. *Mater. Chem. Phys.* **2005**, *92*, 214–219. [[CrossRef](#)]
37. Monti, O.L.A.; Fourkas, J.T.; Nesbitt, D.J. Diffraction Limited Photo generation and Characterization of Silver Nanoparticles. *J. Phys. Chem. B* **2004**, *108*, 1604–1612. [[CrossRef](#)]
38. Osman, M.I.; Abdalla, D.M.; Elfaki, H.A.; Yagoub, Y.A.K.; Ibrahim Hussein, K.; Eldoma, M.A.; Omer Al-atta, N.; Mohamed Osman Siddig, Y. Effects of additive and gamma irradiation on the structural and optical properties of polyvinyl alcohol doped with silver nitrate. *Glob. Sci. J.* **2021**, *9*, 1780–1792.
39. Raouafi, A.; Daoudi, M.; Jouini, K.; Charradi, K.; Hamzaoui, A.H.; Blaise, P.; Farah, K.; Hosni, F. Effect of gamma irradiation on the color, structure and morphology of nickel-doped polyvinyl alcohol films: Alternative use as dosimeter or irradiation indicator. *Nucl. Instrum. Methods Phys. Res. Sect. B Beam Interact. Mater. At.* **2018**, *425*, 4–10. [[CrossRef](#)]

40. Arshak, K.; Korostynska, O.; Harris, J.; Morris, D.; Arshak, A.; Jafer, E. Properties of BGO Thin Films under the Influence of Gamma Radiation. *Thin Solid Film.* **2008**, *516*, 1493–1498. [[CrossRef](#)]
41. Arshak, A.; Zleenti, S.; Arshak, K.  $\gamma$ -Radiation Sensor Using Optical and Electrical Properties of Manganese Phthalocyanine (MnPc) Thick Film. *Sensors* **2002**, *2*, 174–184. [[CrossRef](#)]
42. Eid, S.; Ebraheem, S.; Abdel-Kader, N. Study the Effect of Gamma Radiation on the Optical Energy Gap of Poly (Vinyl Alcohol) Based Ferrotitanium Alloy Film: Its Possible Use in Radiation Dosimetry. *Open J. Polym. Chem.* **2014**, *4*, 21–30. [[CrossRef](#)]
43. Doyan, A.; Susilawati, S.; Prayogi, S.; Bilad, M.R.; Arif, M.F.; Ismail, N.M. Polymer Film Blend of Polyvinyl Alcohol, Trichloroethylene and Cresol Red for Gamma Radiation Dosimetry. *Polymers* **2021**, *13*, 1866. [[CrossRef](#)] [[PubMed](#)]
44. Susilawati, S.; Prayogi, S.; Arif, M.F.; Ismail, N.M.; Bilad, M.R.; Asy'ari, M. Optical Properties and Conductivity of PVA–H<sub>3</sub>PO<sub>4</sub> (Polyvinyl Alcohol–Phosphoric Acid) Film Blend Irradiated by  $\gamma$ -Rays. *Polymers* **2021**, *13*, 1065. [[CrossRef](#)] [[PubMed](#)]
45. Alashrah, S.; El-Ghoul, Y.; Omer, M.A.A. Synthesis and Characterization of a New Nanocomposite Film Based on Polyvinyl Alcohol Polymer and Nitro Blue Tetrazolium Dye as a Low Radiation Dosimeter in Medical Diagnostics Application. *Polymers* **2021**, *13*, 1815. [[CrossRef](#)] [[PubMed](#)]
46. Eldoma, A.M.; Al-atta, N.O.; Ahmed, K.Y. Effect of Doping Concentrations on the Sensitivity of PVA/AgNO<sub>3</sub> Films to low X-ray doses. *Int. J. Adv. Sci. Eng. Technol.* **2019**, *6*, 8460–8466.
47. Lee, H.C. *Introduction to Color Imaging Science*; Cambridge University Press: New York, NY, USA, 2005.
48. Kuehni, R.G. *Color: An Introduction to Practice and Principles*, 2nd ed.; John Wiley: Hoboken, NJ, USA, 2005.
49. Schanda, J. *Colorimetry: Understanding the CIE System*; John Wiley: Hoboken, NJ, USA, 2007.
50. Shams-Nateri, A. Effect of a standard colorimetric observer on the reconstruction of reflectance spectra of coloured fabrics. *Coloration Technol.* **2008**, *124*, 14–18. [[CrossRef](#)]
51. McGrath, J.R.; Beck, M.; Hill, M.E. Replicating Red: Analysis of ceramic slip color with CIELAB color data. *J. Archaeol. Sci. Rep.* **2017**, *14*, 432–438. [[CrossRef](#)]
52. Johnston, W.M.; Kao, E.C. Assessment of Appearance Match by Visual Observation and Clinical Colorimetry. *J. Dent. Res.* **1989**, *68*, 819–822. [[CrossRef](#)]
53. El Gohary, M.I.; Soliman, Y.S.; Amin, E.A.; Gawad, M.H.A.; Desouky, O.S. Effect of perchloric acid on the performance of the Fricke xylenol gel dosimeter. *Appl. Radiat. Isot.* **2016**, *113*, 66–69. [[CrossRef](#)]
54. Abdel-Fattah, A.A.; Beshir, W.B.; Hassan, H.M.; Soliman, Y.S. Radiation-induced coloration of nitro blue tetrazolium gel dosimeter for low dose applications. *Radiat. Meas.* **2017**, *100*, 18–26. [[CrossRef](#)]
55. Emi-Reynolds, G.; Kovacs, A.; Fletcher, J.J. Dosimetry characterization of tetrazolium violet-polyvinylalcohol films. *Radiat. Phys. Chem.* **2007**, *76*, 1519–1522. [[CrossRef](#)]
56. Pikaev, A.K.; Kriminskaya, Z.K. Use of tetrazolium salts in dosimetry of ionizing radiation. *Radiat. Phys. Chem.* **1998**, *52*, 555–561. [[CrossRef](#)]
57. Kovacs, A.; Baranyai, M.; Wojnárovits, L.; Moussa, A.; Othman, I.; McLaughlin, W.L. Aqueous-ethanol nitro blue tetrazolium solutions for high dose dosimetry. *Radiat. Phys. Chem.* **1999**, *55*, 799–803. [[CrossRef](#)]
58. Moussa, A.; Baranyai, M.; Wojnárovits, L.; Kovács, A.; McLaughlin, W. Dosimetry characteristics of the nitro blue tetrazolium-polyvinylalcohol film for high dose applications. *Radiat. Phys. Chem.* **2003**, *68*, 1011–1015. [[CrossRef](#)]
59. Khanna, P.K.; Singh, N.; Charan, S.; Subbarao, V.V.V.S.; Gokhale, R.; Mulik, U.P. Synthesis and characterization of Ag/PVA nanocomposite by chemical reduction method. *Mater. Chem. Phys.* **2005**, *93*, 117–121. [[CrossRef](#)]
60. Ramnani, S.P.; Biswal, J.; Sabharwal, S. Synthesis of silver nanoparticles supported on silica aerogel using gamma radiolysis. *Radiat. Phys. Chem.* **2007**, *76*, 1290–1294. [[CrossRef](#)]
61. Agabekov, V.; Ivanova, N.; Dlugunovich, V.; Vostchula, I. Optical Properties of Polyvinyl Alcohol Films Modified with Silver Nanoparticles. *J. Nanomater.* **2012**, *2012*, 10. [[CrossRef](#)]
62. Eisa, H.W.; Abdel-Moneam, Y.K.; Shaaban, Y.; Abdel-Fattah, A.A.; Zeid, A.M.A. Gamma-irradiation assisted seeded growth of Ag nanoparticles within PVA matrix. *Mater. Chem. Phys.* **2011**, *128*, 109–113. [[CrossRef](#)]
63. Bhat, N.V.; Nate, M.M.; Kurup, M.B.; Bambole, V.A.; Sabharwal, S. Effect of  $\gamma$ -radiation on the structure and morphology of polyvinyl alcohol films. *Nucl. Instrum. Methods Phys. Res. Sect. B Beam Interact. Mater. At.* **2005**, *237*, 585–592. [[CrossRef](#)]
64. Akhavan, A.; Khoylou, F.; Ataeivarjovi, E. Preparation and characterization of gamma irradiated Starch/PVA/ZnO nanocomposite films. *Radiat. Phys. Chem.* **2017**, *138*, 49–53. [[CrossRef](#)]
65. Chen, S.A.; Fang, W.G. Electrically conductive polyaniline-poly (vinyl alcohol) composite films: Physical properties and morphological structures. *Macromolecules* **1991**, *24*, 1242–1248. [[CrossRef](#)]
66. Liu, J.; Lin, Q.; Zhou, Y.; Dai, J.; Han, Y. Shape Controllable Synthesis of Silver Particles by Selecting the Crystallization Routes. *KONA Powder Part. J.* **2020**, *37*, 166–175. [[CrossRef](#)]